Design and synthesis of metal-based chemotherapeutic agents for targeted DNA interactions or DNA repair pathway modulation

Griend, C.J. van de

Chapter 3

Metal-locked helical chirality: inversion barrier and ruthenium-specific asymmetric macrocycle formation

This chapter is published as a full research paper. Corjan van de Griend, Johannes J. van de Vijver, Maxime A. Siegler, Remus T. Dame, and Sylvestre Bonnet. *Inorg. Chem.* **2022**, 61, 40, 16045–16054

Abstract

Upon coordination to metal centers, tetradentate ligands based on the 6,6'-bis(2"-aminopyridyl)-2,2'-bipyridine (H_2babpbpy) structure form helical chiral complexes due to the steric clash between the terminal pyridines of the ligand. For ruthenium(II) complexes, the two additional axial ligands bound to the metal center, when different, generate diastereotopic aromatic protons that can be distinguished by NMR. Based on these geometrical features, the inversion barrier of helical $[Ru^{II}(L)(RR'SO)Cl]^+$ complexes, where L is a sterically hindered tetrapyridyl H_2babpbpy derivative, and RR'SO a chiral or achiral sulfoxide ligand, were studied by variable-temperature ^{1}H NMR. The coalescence energies for the inversion of the helical chirality of [Ru(H_2babpbpy)(DMSO)(Cl)]Cl and [Ru(H_2babpbpy)(MTSO)(Cl)]Cl (where MTSO (*R*)-methyl p-tolylsulfoxide) were found to be 43 kJ/mol and 44 kJ/mol, respectively. By contrast, in [Ru(H_2biqbpy)(DMSO)(Cl)]Cl (H_2biqbpy = bis(aminoquinoline)bipyridine), increased strain caused by the larger terminal quinoline groups resulted in a coalescence temperature higher than 376 K, which pointed to an absence of helical chirality inversion at room temperature. Further increasing the steric strain by introducing methoxy groups ortho to the nitrogen atoms of the terminal pyridyl groups in H_2babpbpy, resulted in the serendipitous discovery of a ring-closing reaction that took place upon trying to make $[Ru(OMe\text{-}H_2babpbpy)(DMSO)Cl]^+$. This reaction generated, in excellent yields, a chiral complex [Ru(L")(DMSO)Cl]Cl where L" is an asymmetric tetrapyridyl macrocycle. This unexpected transformation appears to be specific to ruthenium(II), as macrocyclization did not occur upon coordination of the same ligand to palladium(II) or rhodium(III).

3.1 Introduction

The interaction between inorganic compounds and biomolecules such as proteins or nucleic acids has been widely studied[1–7] since the discovery of the anticancer properties of cisplatin.[8,9] Especially the interaction with DNA has gathered wide attention[10,11] as more and more platinum-based analogues of cisplatin have been reported, with improved properties such as oxaliplatin or satraplatin.[12] One method to generate specific interaction between inorganic compounds and DNA is to use chiral scaffolds. Octahedral metal complexes have the potential to be chiral and several synthetic routes have been reported, where one enantiomer of an inorganic compound is enriched or even a single enantiomer is selectively formed.[13,14] These chiral complexes offer improved characteristics in relation to DNA binding such as higher DNA binding constants,[15,16] increased luminescence quantum yields upon binding onto DNA, higher degree of DNA photocleavage,[17–19] or improved threading intercalation into DNA.[20] One notable compound is $[Ru(bpy)_2(dppz)]^{2+}$, which was originally reported by the group of Barton for its "light switch" properties. This chiral complex is non-emissive in water, but becomes luminescent upon intercalation of the dppz moiety into double-stranded

DNA.[21] Later work reported improved luminescence for the delta enantiomer upon binding to mismatch DNA, while the lambda enantiomer showed preference for abasic sites.[22]

So far, most chiral complexes discussed in the bioinorganic literature relate to point chirality, where the stereogenic center is either the metal atom itself, and/or one of the carbon atoms of a ligand. Other forms of chirality, however, exist. For example, helical chirality offers a fascinating range of compounds known in organic chemistry as helicenes; their properties have been reviewed comprehensively elsewhere.[23,24] Helicenes consist of ortho-fused aromatic rings that cannot adopt a flat planar conformation due to the steric hindrance of the terminal rings; these molecules therefore adopt a helical structure, which is inherently chiral and can exist as two enantiomers noted P and M.[25] The inversion barrier between these two forms rapidly increases upon extension of the aromatic system with activation energies of 96.3 kJ/mol for [5]Helicene[26] and 151.5 KJ/mol for [6]Helicene.[27] A recent trend in this field is the coordination of helicene-containing ligands to metal centers, which has been shown to alter the properties of the helicenes.[28–30] For example, the coordination of helical ligands to iridium compounds resulted in a light-green phosphorescence with unusually long lifetimes. Recently, the group of Crassous reported the synthesis and structural characterization of a range of helicene-like ligands coordinated to ruthenium, forming metal complexes based on the $[Ru(bpy)_3]^{2+}$ scaffold, but with an extended π conjugation system.[31] The same group even reported the synthesis and crystal structure of a enantio-enriched binuclear ruthenium complex linked by a helical ligand containing two bpy-like moieties. Another type of helical-chiral metal complexes are those based on the non-chiral 6,6'-bis(2"-aminopyridyl)-2,2'-bipyridine ligand (H_2babpbpy).[32] Upon metal coordination, this type of ligands can no longer adopt a flat conformation due to the steric clash between its terminal pyridines, which imposes a helical conformation to the tetrapyridyl structure (Figure 1). Typically, single crystal X-ray structures of these helicenoid complexes show both helical enantiomers present in the crystal lattice.[31] As we recently found that H_2babpbpy-based ruthenium[33,34] or platinum[35] complexes can interact with DNA, and considering that the ease at which chiral inversion of the helix occurs had remained up to now unknown, we engaged in this work into determining the barrier of inversion of the helical chirality of such molecules.

Considering that the helicity of these complexes is a direct consequence of the steric strain between the terminal pyridyl groups of the H_2babpbpy ligand, we synthesized ruthenium(II) H_2babpbpy-based derivatives with varying levels of steric strain on these terminal pyridines (Figure 2), and studied the interconversion between the two helical enantiomers using variable temperature ^{1}H NMR. We explored this helical inversion both on chiral complexes of the type [Ru(L)(DMSO)Cl]Cl ([**1**]Cl and [**2**]Cl, with L = H_2babpbpy

or L = 6,6'-bis(aminoquinoline)-2,2'-bipyridine = H_2biqbpy, respectively, where DMSO is the non-chiral ligand dimethylsulfoxide, and on their analogues [Ru(L)(MTSO)Cl]Cl ([**3**]Cl-[**4**]Cl with L= H_2bapbpy and H_2biqbpy, respectively) and [Ru(H_2biqbpy)(EtOHPy)$_2$] (PF_6)$_2$ ([**5**](PF_6)$_2$), where MTSO and EtOHPy are the enantiomerically pure chiral ligands (*R*)-methyl p-tolylsulfoxide and (*R*)-(+)-α-methyl-4-pyridinemethanol, respectively. In the latter cases, the enantiopure nature of the axial ligand(s) generates diastereomers upon coordination to the helical-chiral complexes that can be distinguished by NMR. Finally, we report the serendipitous discovery of a macrocyclization reaction taking place when the most sterically hindered ligand of the series, L=6,6'-bis(6-methoxy-aminopyridyl)-2,2'-bipyridine (OMe-H_2bapbpy), was coordinated to ruthenium(II).

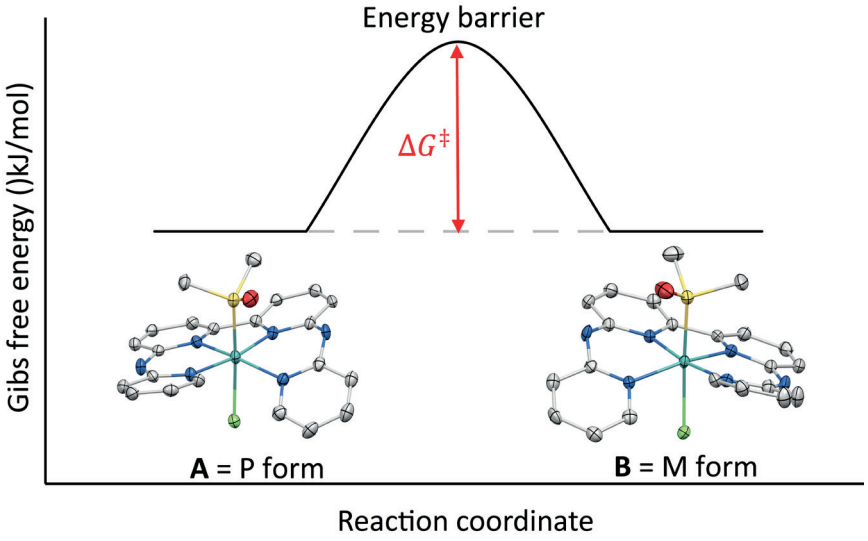

Figure 1. Graphical representation of the coalescence energy ($\Delta G^{\ddagger}$) for the inversion of the helical chirality of [Ru(H_2bapbpy)(DMSO)(Cl)]$^+$.

3.2 Results

The achiral tetradentate H_2bapbpy and H_2biqbpy ligands were reacted with the precursor [Ru(DMSO)$_4$Cl$_2$] to form racemic mixtures of the chiral complexes [**1**]Cl and [**2**]Cl, respectively. This reaction was achieved by a straightforward overnight reflux at 80 °C in ethanol in 68% and 96% yield, respectively. The DMSO axial ligand was further substituted by an enantiomeric pure sulfoxide ligand MTSO to afford mixtures of diastereoisomer complexes of compounds [**3**]Cl and [**4**]Cl, respectively. To complete our investigations on the chirality of these structures, we finally substituted both axial ligands by the chiral pyridine EtOHPy to afford compound [**5**](PF_6)$_2$ as a mixture of epimers (*P*,*R*,*R* and *M*,*R*,*R*) that differ in only one stereo center.

Single crystals suitable for X-ray structure determination for [**3**]PF_6 and [**5**]$(PF_6)_2$ were obtained by vapor diffusion of diethylether into a methanol solution containing the metal compound (0.2 mg/mL), in presence or in absence, respectively, of a drop of 55% HPF_6 in water. The crystal structures are shown in Figure 3 and a selection of bond lengths and angles is reported in Table 1. Both structures show the chiral helically distorted conformation of the tetradentate ligand. The crystal lattice of [**3**]PF_6 contains both the (P,R) and (M,R) diastereomers and in [**5**]$(PF_6)_2$ both the (P,R,R) and (M,R,R) epimers are present (figure SII.1). The N1N3N4N6 dihedral angle, which is one measure of the helical distortion, is 9.9(6)° for [**3**]$^+$ and 16.6(4)° for [**5**]$^{2+}$. Clearly, the extended aromatic system of the H_2biqbpy ligand, compared to H_2bapbpy, results in an increase of the helical distortion of the ligand upon coordination to ruthenium(II).

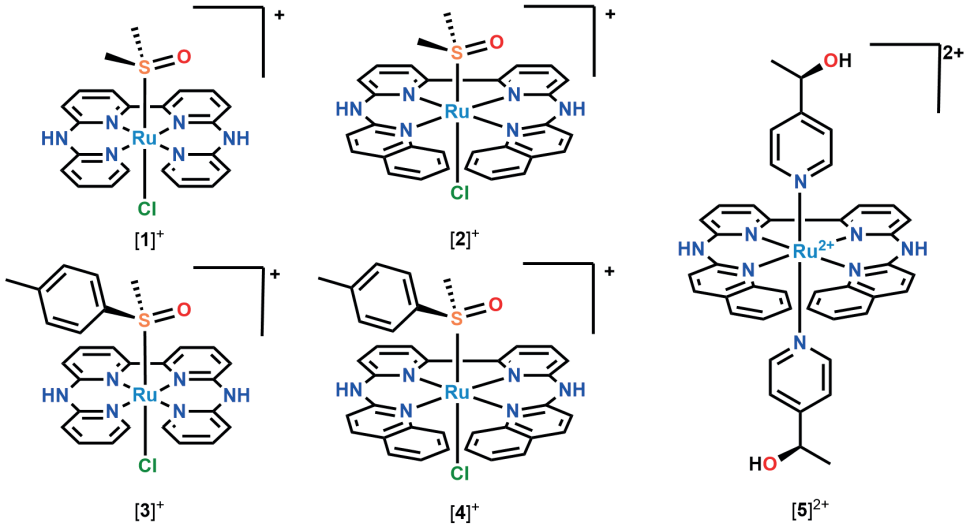

Figure 2. Chemical structure of the compounds used in the helical inversion ^{1}H-NMR study.

The room-temperature ^{1}H NMR spectra of the ruthenium complexes already offer an intriguing insight into their chiral structure and dynamics (Figure 4). The helical-chiral, racemic complex [**1**]Cl showed only 7 aromatic signals, indicating that at the NMR time scale this complex has an average plane of symmetry perpendicular to the average plane of the babpbpy ligand. By contrast, upon substitution of the non-chiral axial DMSO ligand by the chiral, enantiomerically pure MTSO ligand, all aromatic signals assigned to the H_2bapbpy ligand are doubled in [**3**]Cl, which is consistent with the formation of diastereotopic protons, while the two aromatic MTSO signals indicate the presence of only one species. Overall, the doubling of the babpy-based proton peaks in [**3**]$^+$ can be attributed to the loss of the plane of symmetry in the complex concomitant to the substitution of the achiral sulfoxide DMSO by the chiral MTSO. The fact that one single species is observed in the room temperature ^{1}H-NMR spectrum of [**3**]Cl,

while its crystal structure contains both diastereoisomers, leads to the conclusion that the helicity inversion due to the switching of the position of the terminal pyridines is rapid on NMR time scales at room temperature, rendering the separation of these diastereomers impossible.

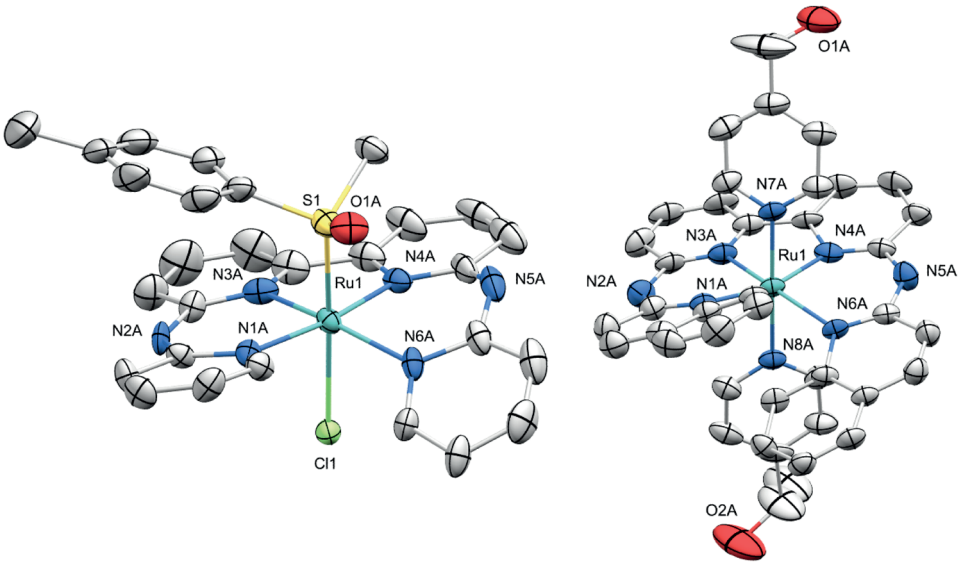

[**3**]$^{+}$ [**5**]$^{2+}$

Figure 3. Displacement ellipsoid plots (50% probability level) for [**3**]PF_6 and [**5**]$(PF_6)_2$ at 110(2) K. Counter ions and hydrogens have been omitted for clarity.

Interestingly, the H_2biqbpy analogue [**2**]Cl showed 18 aromatic signals at room temperature in solution, indicating that, unlike [**1**]Cl, this complex has no average plane of symmetry: the chemical environment of the terminal quinolines on the side of the DMSO vs. chlorido axial ligands i) are different enough to be distinguished, and ii) cannot exchange on NMR time scale at room temperature. In other words, each pair of protons of the H_2biqbpy ligand that are equivalent by symmetry in the free ligand, and would remain equivalent in a hypothetical planar conformation tetracoordinated to a metal center, become diastereotopic in the real, helical complex. In absence of rapid exchange of the helicity of the complex, they can be distinguished by NMR. H_2Biqbpy has hence increased strain, compared to H_2bapbpy, with regard to helix inversion, which can be interpreted as a cause of the larger size of the quinoline groups, compared to pyridine groups in [**1**]$^{+}$. The substitution of the achiral DMSO ligand in [**2**]$^{+}$ by the chiral sulfoxide MTSO, to give [**4**]$^{+}$, led according to ^{1}H NMR to the formation of one major and one minor diastereoisomer, with a diastereoisomeric excess of ~50. The symmetry is here as well very low, which suggests the absence of inversion of the helix at room temperature. For example, 4 amine peaks can be clearly distinguished near 11.6 ppm.

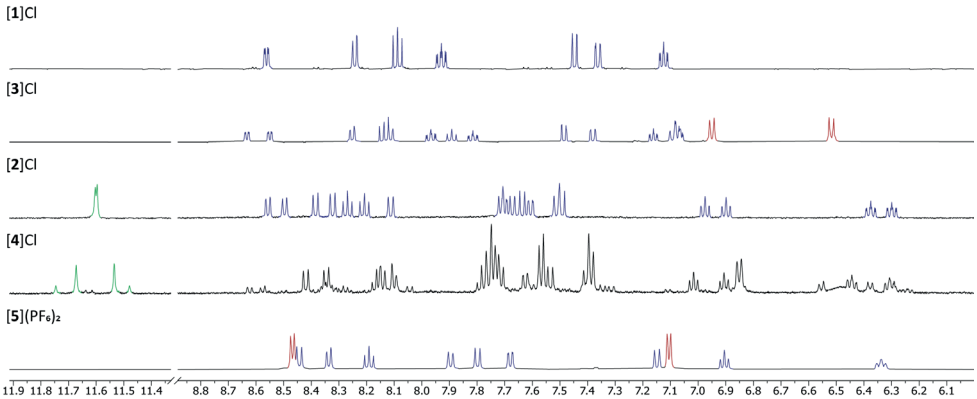

Figure 4. ^{1}H NMR spectra of [**1**]$^{+}$ and [**3**]$^{+}$ in methanol-*d4*, [**2**]$^{+}$ and [**4**]$^{+}$ in DMSO-*d6* and [**5**]$^{2+}$ in acetone-*d6*. The blue colored peaks are assigned to the tetradentate ligands, the red peaks to the chiral ligand, the green peaks to the bridging amine and the black peaks are unassigned.

As a note, diastereomers are distinct species with *a priori* different physical properties that one expects to be separable on achiral HPLC columns. Disappointingly, we were unable to separate these two diastereoisomers, neither on an achiral preparative nor on a chiral semi-prep Astec® CYCLOBOND I 2000 DMP column. The labile chlorido ligand proved problematic as it rapidly hydrolyzes by the aqueous component of the HPLC eluents, and further substituted by MeCN, effectively rendering any eluents containing H_2O or MeCN dysfunctional. Other eluent systems were tried but did not yield the desired separation. Still, we were able to identify two species when an analytical sample was measured on the chiral semi-prep DMP column, with 0.1 M NH_4Cl in MeOH as eluent, as seen in Figure SII.2. Finally, in the NMR spectrum of [**5**]$(PF_6)_2$ (Figure 3), only 9 peaks are assigned to the H_2biqbpy ligand, and 2 peaks to the axial pyridines (EtOHPy), as the complex has a C2 rotational symmetry axis. Each molecule has 3 chiral centers and the crystal structure shows the presence of both the P and M epimers. While at a first glance the ^{1}H NMR seemed to show only one species in the aromatic region, in the aliphatic region, it shows 2 doublets overlapping at 1.09 ppm, which are assigned to diastereomer methyl groups of the coordinated EtOHPy. The ^{13}C NMR spectrum also showed two peaks almost overlapping at 65.7 ppm for the CH chiral carbon atom of the axial ligands. These results confirm the formation of two closely related epimers, even though the chiral centers are too far apart to directly influence each other, and most aromatic signals for the epimers seem to overlap. Also in this case, the separation of these two epimers could not be achieved.

Clearly, upon coordination to the metal, the helicity of the H_2bapbpy ligand switches back and forth quickly at room temperature, while that of H_2biqbpy is blocked. To measure the inversion barriers for both types of structures, variable temperature ^{1}H NMR spectra were recorded for compounds [**1**]$^{+}$, [**2**]$^{+}$ and [**3**]$^{+}$ (Figure 5). The spectra of [**1**]$^{+}$ and [**3**]$^{+}$ showed a doubling of the number of peaks as the temperature decreased.

Thus, as the temperature was lowered the interconversion of both terminal pyridines in the helical complexes became slow, compared to NMR timescales, leading to vanishing of the average plane of symmetry of the H_2bapbpy ligand in both enantiomers, and to the observation of 1:1 pairs of diastereoisomeric H_2bapbpy protons for compound [**1**]$^+$. For compound [**3**]$^+$, the same phenomenon resulted in the blocking of the interconversion of the two diastereomers, below which their protons became distinguishable as well. The integrals of both diastereoisomers are roughly 1:1, showing that these diastereomers have similar free Gibbs energies. The coalescence energy of [**1**]$^+$ was found to be 43 kJ/mol, determined from the doublet at 8.25 ppm and a corresponding coalescence temperature of 206 K.[36] For compound [**3**]$^+$, 44 kJ/mol was found from the singlet at 2.5 ppm and a coalescence temperature of 216 K. Both values are significantly lower than the 96.3 kJ/mol reported for [5]Helicine, demonstrating that comparatively very rapid interconversion occurs at room temperature. The contribution of the different sulfoxide is minimal, which indicated that the coalescence energy is mainly determined by the size of the pyridyl group, and not by the size of the sulfoxide substituents.

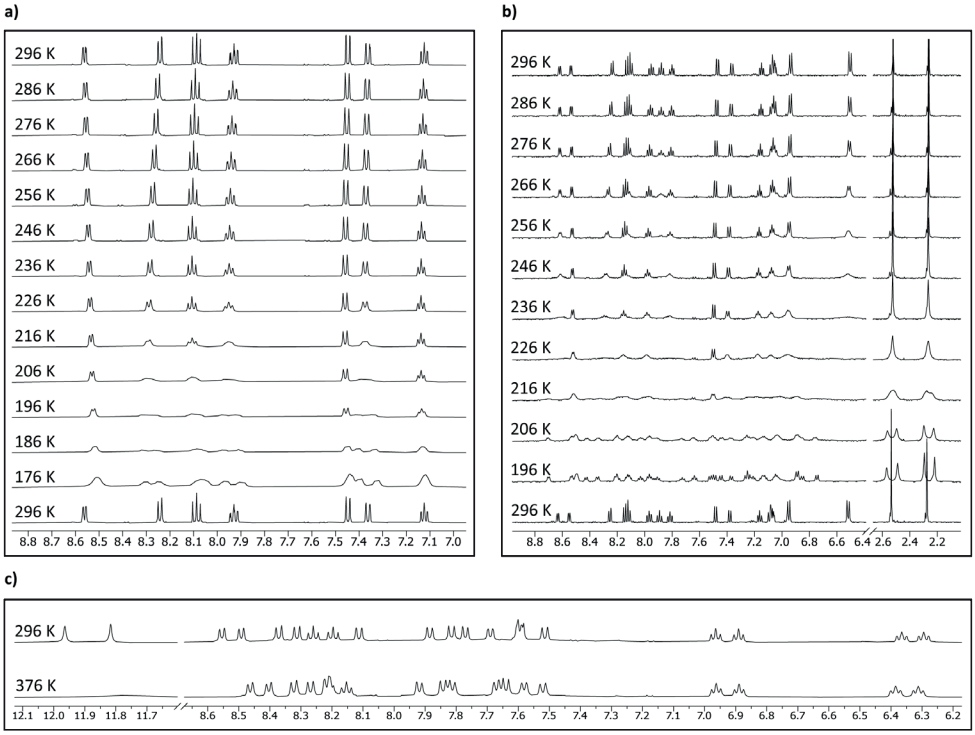

Figure 5. a) Variable-temperature ^{1}H NMR of [**1**]$^+$ in methanol-*d4* from 296 K to 176 K. b) [**3**]$^+$ in methanol-*d4* from 296 K to 196 K. c) [**2**]$^+$ in DMSO-*d6* from 296 K to 379 k.

For compound [**2**]$^+$ the coalescence temperature was dramatically increased, compared to that of [**1**]$^+$ and [**3**]$^+$. When the temperature was increased up to 376 K, which was the limit of our spectrometer, 18 diastereotopic protons could still be seen, pointing

to an absence of exchange of the terminal quinolines even at such high temperatures. Overall, the increased size of the quinolyl groups in [**2**]$^+$ resulted in a significant increase in the coalescence energy of this complex, compared to [**1**]$^+$. This coalescence energy must be higher than 79 kJ/mol, which is the value calculated based on the chemical shift of the two triplets at 6.37 ppm and 6.29 ppm and a coalescence temperature of 376 K.

Attempts to prepare a helical compound with increased steric strain generated by methoxy groups in ortho position to the N atoms of the terminal pyridyl groups of H_2bapbpy produced unexpected results. When reacting OMe- H_2bapbpy with [Ru(DMSO)$_4$Cl$_2$] in the same conditions as that used to make [**1**]Cl and [**3**]Cl, a solid was obtained ([**6**]Cl) that could initially not be identified based on ^{1}H NMR. Single crystals suitable for X-ray structure determination were obtained, which allowed identification of the product (Figure 6). According to this crystal structure, the product resulted not only from ligand coordination, but also from a subsequent ring-closing reaction, which is accompanied by the removal of one of the methoxy groups, and the methylation of one of the bridging amines. In the X-ray structure of [**6**]OTf, a dissymmetric macrocycle (macro) ligand is coordinated to ruthenium, with four symmetry-unequivalent pyridyl rings (Scheme 1). This structure was further confirmed by NMR and HRMS ([M+MeCN–2Cl-H]$^+$ calc m/z = 588.07510, found m/z = 588.07561) analyses of the product (see full characterization in the Experimental Part). This reaction is robust and reproducible, affording the macrocycle in high yield (~75 %). We hypothesize the following mechanism for the formation of the macrocycle in [**6**]$^+$. The close proximity of the two facing methoxy groups arising from the coordination of the OMe-H_2bapbpy ligand to ruthenium(II) might facilitate an intramolecular nucleophilic aromatic substitution via an oxonium ion intermediate, which would subsequently transfer a methyl group, probably in a bimolecular reaction, to the facing amine bridge, thereby forming the final dissymmetric macrocycle.

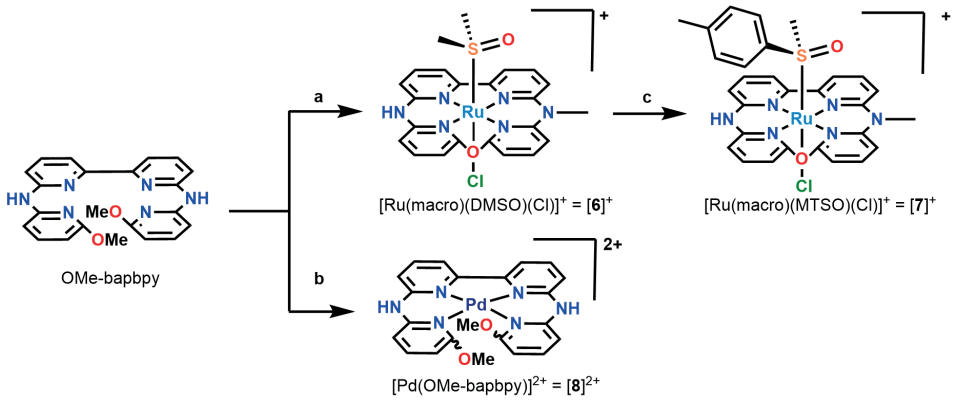

Scheme 1. Synthetic route towards compounds [**6**]$^+$, [**7**]$^+$, and [**8**]$^{2+}$. a) [Ru(DMSO)$_4$(Cl)$_2$], EtOH, 85 °C. b) [Pd(1,5-Cyclooctadiene)Cl$_2$], EtOH, 85 °C. c) MTSO, MeOH, 75 °C.

The dissymmetric nature of the macrocycle om [**6**]$^{+}$ also caused the ruthenium complex to be chiral-at-metal, as the metal center is bound in this structure to 6 non-equivalent heteroatoms. In the crystal structure of [**6**]OTf, both enantiomers are found as the structure is centrosymmeteric. When the chiral sulfoxide MTSO ligand was coordinated to scaffold [**6**]Cl, to afford [**7**]Cl, the number of peaks in the ^{1}H NMR spectrum of [**7**]Cl roughly doubled, which is consistent with the dissymmetric nature of the ring and the formation of a 1:1 mixture of diastereoisomers. Although we were unable to separate these diastereoisomers, we did obtain a crystal structure of [**7**](OTf)(MeOH) (Figure 6), which also showed the presence of both diastereoisomers in the crystal packing. As a note, dissymmetric macrocyclic ligands have been reported in particular for preparing chiral catenanes and other topologically non-obvious mechanically interlocked molecules,[37,38] but they are often challenging to make. Here the macrocycle is obtained in a straightforward manner and in good yields, though the presence of the coordinated ruthenium center prevents threading of any molecular building block into the ring.

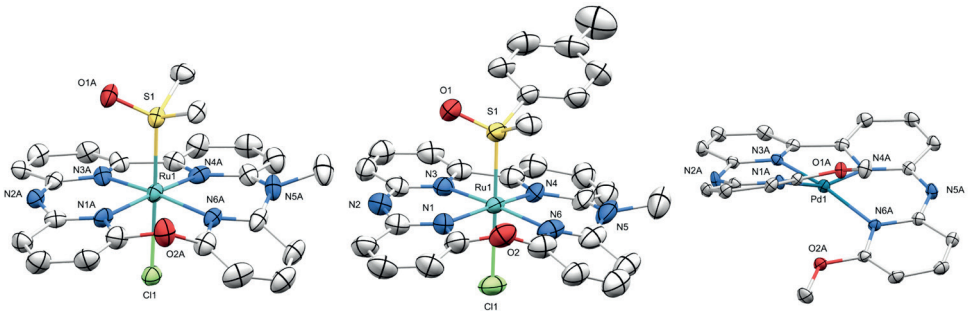

[**6**]$^{+}$ [**7**]$^{+}$ [**8**]$^{2+}$

Figure 6. Displacement ellipsoid plots (50% probability level) of the crystal structures of [**6**]OTf, [**7**](OTf). MeOH, and [**8**](OTf)$_2$ at 110.(2) K. Counter ions, hydrogens and solvents molecules have been omitted for clarity.

Finally, to further investigate the role of the metal in this unexpected cyclization reaction, we investigated the coordination of the OMe- H_2bapbpy ligand to the palladium(II) precursor dichloro(1,5-cyclooctadiene)platinum(II) using otherwise identical reaction conditions. Palladium(II) is a d^8 metal center usually affording square-planar complexes deprived of axial ligands. Surprisingly, this reaction resulted in the simple coordination of the tetrapyridyl ligand to the complex without ring closure, to afford complex [**8**]$^{2+}$. The identity of complex [**8**]$^{2+}$ is supported by NMR, mass (ES-MS [Pd(OMe- H_2bapbpy)-H^{+}]$^{+}$ calc m/z = 505.0, found m/z 504.9), and single crystal X-ray crystallography of [**8**](OTf)$_2$ (Figure 6), which clearly showed an increase in helical strain caused by the terminal methoxy groups, with a N1N3N4N6 dihedral angle of 20.8(9)° that is twice higher that that found for the archetypal H_2bapbpy complex

[**2**]$^{+}$. Even though macrocycle formation did not occur with palladium(II), this crystal structure also demonstrated the close spatial proximity between the two methoxy groups upon binding of the 4 pyridyl groups to the metal, with a O1-O2 distance between the "top" oxygen O1 and "bottom" oxygen O2 of 3.01(7) Å. To see if the axial ligands of the ruthenium(II) precursor are pivotal in the macrocycle formation, we also reacted the OMe-H_2bapbpy ligand with a Rh(III) precursor ($RhCl_3$ $3H_2O$) in otherwise identical conditions. Here as well, ^{1}H NMR and ESI mass spectrometry of the product showed simple coordination of the ligand to rhodium(III) (ES-MS [Rh(OMe-H_2bapbpy)$(Cl)_2$]$^{+}$ calc m/z = 573.0, found m/z =572.9), without formation of any macrocycle. This result indicated that it is not only the presence of the axial ligands on ruthenium(II) that facilitates macrocycle formation in [**6**]$^{+}$, but that the macrocyclization reaction is specific to the reactivity of ruthenium(II).

Table 1. Selected bond distances (Å) and angles (°) found in the crystal structures of [**3**]PF_6, [**5**]$(PF_6)_2$, [**6**]OTf, [**7**](OTf).MeOH, and [**8**]$(OTf)_2$

Compound	[**3**]$^{+,b}$	[**5**]$^{2+,c}$	[**6**]$^{+,b}$	[**7**]$^{+}$	[**8**]$^{2+,b}$
M-N1	2.098(9)	2.146(8)	2.089(7)	2.123(9)	2.078(2)
M-N3	2.031(9)	2.023(8)	2.033(6)	2.027(10)	2.065(2)
M-N4	2.022(8)	2.020(8)	2.031(7)	2.012(9)	1.991(2)
M-N6	2.102(9)	2.180(8)	2.051(6)	2.089(11)	1.977(2)
M-S1	2.207(2)	-	2.214(2)	2.192(3)	-
M-Cl1	2.430(2)	-	2.421(2)	2.456(3)	-
C1-O2-C20	-	-	124.9(7)	127.1(10)	-
C5-N2-C6	135.5(9)	132.0(5)	134.9(7)	136.6(10)	130.3(3)
C15-N5-C16	130.3(3)	132.5(9)	127.8(7)	131.6(11)	132.5(3)
N1-M-N4	172.5(3)	165.3(3)	171.2(3)	168.6(4)	162.15(10)
N3-M-N6	165.1(3)	167.7(3)	169.8(3)	173.4(8)	165.34(10)
τ_4[a]	0.1(6)	0.1(9)	0.1(3)	0.1(3)	0.2(3)
Torsion angle N1-N3-N4-N6	10.8(4)	16.6(4)	1.2(2)	1.4(0)	20.8(9)

[a] The coordination angles N1-M1-N4 and N3-M1-N6 are used to calculate τ_4.[39] $\tau_4 = \frac{360 - (\alpha + \beta)}{141}$

[b] Consists of two crystallographically independent formular units for the structure. The bond distance and angles are given for molecule A.

[c] Consists of four crystallographically independent formular units for the structure. The bond distance and angles are given for molecule A

3.3 Conclusion

In this work, we report the synthesis of helical ruthenium compounds with varying levels of steric strain induced by substituents located ortho to the terminal pyridyl rings of H_2bapbpy-like ligands. The coordination of an enantiomerically pure (*R*)-sulfoxide axial ligand confirmed that the terminal pyridines of [**3**]$^+$ can freely interconvert at room temperature. Variable-temperature NMR allowed the determination of coalescence temperature and energy for both complexes [**1**]$^+$ and [**3**]$^+$ (43 and 44 kJ/mol, respectively). In [**2**]$^+$, the terminal quinolines cannot exchange position at room temperature, and heating up to 376 K did not allow to overcome such steric clash. Coordination of the chiral sulfoxide ligand MTSO led to the formation of one major and one minor species, but they could not be separated on HPLC, essentially due to the labile character of the *trans* chlorido ligand. Finally, we report the serendipitous discovery of a robust macrocycle-forming reaction when the methoxy-functionalized OMe-H_2bapbpy ligand was reacted with ruthenium(II). This reactivity is specific to ruthenium(II), as palladium(II) and rhodium(III) precursors did not result in macrocycle formation but instead led to the simple coordination of the OMe-H_2bapbpy ligand.

3.4 Experimental part

3.4.1 Synthesis

All commercially available reagents were ordered from Sigma-Aldrich and were used as received. H_2Bapbpy[32], H_2biqbpy[40], (*R*)-Methyl p-tolyl sulfoxide (MTSO)[41], and compound [**1**]Cl[33] were prepared according to literature procedures. All reactions were carried out under a N_2 atmosphere. Filters used were Whatman® regenerated cellulose membrane filters, RC60 Membrane Circles, diam. 47 mm, pore size 1 µm. NMR spectra were recorded on a Bruker, AV-500 spectrometer. HPLC purifications were attempted on the non chiral column Jupiter 4u Protea 90A, ASXIA and chiral CYCLOBOND I 2000 DMP column. Electrospray ionization mass spectra (ESI-MS) were recorded by using a MSQ Plus Spectrometer positive ionization mode. High resolution mass spectra (HRMS) were recorded on Waters XEVO-G2 XSQ-TOF) mass spectrometer equipped with an electrospray ion source in positive mode (source voltage 3.0 kV, desolvation gas flow 900 L/hr, temperature 250 °C) with resolution R= 22000 (mass range m/z = 50-2000) and 200 pg/uL Leu-enkephalin (m/z = 556.2771) as a “lock mass”.

3.4.1.1 6-OMeH_2bapbpy

6,6’-dibromo-2,2’-bipyridine (3.0 g, 10 mmol), Pd(dba)2 (295 mg, 0.51 mmol), (Rac)-BINAP (500 mg, 0.80 mmol) and potassium *t*-butoxide (4.2 g, 38 mmol) were added to a flask containing toluene (300 mL). Afterwards, 2-amino-6-methoxypyridine (3.1 mL, 29 mmol) was added and the reaction was refluxed overnight at 110 °C. The next day the reaction was allowed to cool down to room temperature, after which water (150

mL) was added. The mixture was stirred for 1 h, after which it was filtered and the solid washed with water (2x 25 mL). The solid residue was finally dried under vacuum to afford the title compound as a beige colored solid. Yield: 3.6 g, 8.9 mmol, 90%. **^{1}H NMR** (500 MHz, DMSO) δ 9.66 (s, 2H), 7.89 – 7.80 (m, 4H), 7.75 (d, J = 6.7 Hz, 2H), 7.64 (t, J = 7.9 Hz, 2H), 7.49 (d, J = 7.9 Hz, 2H), 6.31 (d, J = 7.9 Hz, 2H), 3.89 (s, 6H). **^{13}C NMR** (126 MHz, DMSO) δ 162.36 (Cq), 153.69 (Cq), 153.53 (Cq), 152.49 (Cq), 140.39 (CH), 138.33 (CH), 112.43 (CH), 112.08 (CH), 103.10 (CH), 100.70 (CH), 53.02 (CH_3). **HRMS** $[M+H]^+$: 401.17205 (calculated) 401.17204 (measured)

3.4.1.2 [2]Cl

H_2biqbpy (90 mg, 0.21 mmol) and $[Ru(DMSO)_4(Cl)_2]$ (0.10 g, 0.21 mmol) was dissolved in degassed ethanol (25 mL). The solution was refluxed for 3 days at 80 °C under N_2 atmosphere. The mixture was concentrated in vacuo and reprecipitated from MeOH (5 mL) with diethyl ether (50 mL) afford the title compound [**3**]Cl as a dark brown powder. Yield: 0.15 g, 0.20 mol, 96%. **^{1}H NMR** (500 MHz, DMSO) δ 12.31 (s, 1H), 12.08 (s, 1H), 8.55 (d, J = 6.9 Hz, 1H), 8.49 (d, J = 6.9 Hz, 1H), 8.36 (d, J = 8.8 Hz, 1H), 8.30 (d, J = 8.8 Hz, 1H), 8.25 (t, J = 8.0 Hz, 1H), 8.18 (t, J = 8.0 Hz, 1H), 8.12 (d, J = 8.8 Hz, 1H), 8.05 (d, J = 8.3 Hz, 1H), 7.99 (d, J = 8.9 Hz, 1H), 7.90 (d, J = 7.2 Hz, 1H), 7.72 (d, J = 8.8 Hz, 1H), 7.68 (dd, J = 7.9, 1.6 Hz, 1H), 7.59 (dd, J = 7.8, 1.7 Hz, 1H), 7.52 (d, J = 8.8 Hz, 1H), 6.96 (t, J = 7.4 Hz, 1H), 6.88 (t, J = 6.8 Hz, 1H), 6.36 (ddd, J = 8.6, 6.9, 1.6 Hz, 1H), 6.29 (ddd, J = 8.8, 6.9, 1.6 Hz, 1H), 2.54 (s, 6H). **^{13}C NMR** (126 MHz, DMSO) δ 156.91 (Cq), 155.85 (Cq), 154.37 (Cq), 153.01 (Cq), 151.24 (Cq), 150.66 (Cq), 148.55 (Cq), 148.37 (Cq), 138.78 (CH), 138.52 (CH), 137.96 (CH), 137.02 (CH), 130.55 (CH), 129.11 (CH), 128.01 (CH), 127.68 (CH), 126.72 (CH), 126.63 (CH), 124.78 (Cq), 124.51 (Cq), 124.37 (CH), 123.96 (CH), 118.08 (CH), 117.55 (CH), 116.07 (CH), 115.90 (CH), 115.00 (CH), 113.87 (CH), 40.36 (CH_3). **HRMS** [M+MeCN–2Cl-DMSO]2+: 291.55277 (calculated) 291.55249 (measured). **Elem. Anal.** Calcd. For $[C_{30}H_{28}Cl_2N_6O_2RuS] + H_2O$: C, 50.85; H, 3.89; N, 11.86. Found: C, 50.72; H, 3.73; N, 11.69.

3.4.1.3 [3]Cl

[**1**]Cl (30 mg, 0.051 mmol) and (R)-methyl(p-tolyl)sulfoxide (MTSO) (0.21 g, 1.3 mmol) were added to degassed methanol (10 mL). The solution was refluxed overnight, after which the solution was allowed to cool to room temperature and precipitated by addition of diethyl ether (10 mL). The precipitate was filtered, washed with diethyl ether (2 x 50 mL) and dried under vacuum to afford the desired compound as a red brown colored solid. Yield: 37 mg, 0.051 mmol, 100%. **^{1}H NMR** (500 MHz, DMSO) δ 11.66 (s, 1H), 11.13 (s, 1H), 8.44 (dd, J = 6.1, 1.7 Hz, 1H), 8.37 (dd, J = 6.1, 1.7 Hz, 1H), 8.29 (dd, J = 7.9, 1.0 Hz, 1H), 8.18 – 8.06 (m, 2H), 7.95 (ddd, J = 8.6, 7.1, 1.7 Hz, 1H), 7.89 (t, J = 8.0 Hz, 1H), 7.80 (ddd, J = 8.6, 7.0, 1.7 Hz, 1H), 7.69 (d, J = 7.3 Hz, 1H), 7.58 (dd, J = 8.5, 1.4 Hz, 1H), 7.29 – 7.22 (m, 2H), 7.13 (ddd, J = 7.3, 6.1, 1.4 Hz, 1H), 7.04

(ddd, J = 7.3, 6.0, 1.4 Hz, 1H), 6.87 (d, J = 8.0 Hz, 2H), 6.42 (d, J = 8.3 Hz, 2H), 2.43 (s, 3H), 2.21 (s, 3H). **^{13}C NMR** (126 MHz, DMSO) δ 155.67 (Cq), 155.22 (Cq), 153.06 (CH), 153.01 (CH), 152.66 (Cq), 152.25 (Cq), 151.12 (Cq), 150.37 (Cq), 140.59 (Cq), 140.34 (Cq), 138.01 (CH), 137.61 (CH), 137.47 (CH), 136.83 (CH), 128.69 (CH), 122.71 (CH), 117.13 (CH), 117.01 (CH), 116.79 (CH), 114.57 (CH), 114.40 (CH), 114.11 (CH), 114.03 (CH), 43.78(CH_3), 20.66 (CH_3). **HRMS** [M+MeCN–2Cl-H]$^+$: 636.11250 (calculated) 636.11207 (measured). **Elem. Anal**. Calcd. For [$C_{28}H_{28}Cl_2N_6O_2RuS$] + H_2O: C, 49.12; H, 4.12; N, 12.28. Found: C, 49.13; H, 4.13; N, 12.27.

3.4.1.4 [4]Cl

[**2**]Cl (42 mg, 0.08 mmol) and (R)-methyl p-tolylsulfoxide MTSO (0.17 g, 1.1 mmol) were added to degassed methanol (15 mL). The solution was refluxed for 3 days at 75 °C under N_2 atmosphere. After concentration in vacuo the solid residue was sonicated in ethyl acetate (15 mL) and filtered and washed with diethyl ether (2 x 50 mL) to obtain the title compound [**4**]Cl as dark brown powder. Yield: 45 mg 0.06, 75 %. **HRMS** [M-2Cl-H]$^+$: 695.11704 (calculated) 695.11677 (measured). **Elem. Anal**. Calcd. For [$C_{36}H_{30}Cl_2N_6ORuS$] : C, 56.40; H, 3.94; N, 10.96. Found: C, 56.28; H, 3.93; N, 10.94.

3.4.1.5 [5]$(PF_6)_2$

[**2**]Cl (53 mg, 0.08 mmol) and (*R*)-4-(1-hydroxyethyl)pyridine (0.45 g, 3.6 mmol) were added to a flask containing deoxygenated demineralized water (45 mL). The solution was stirred for 1 day at 80 °C under N_2 atmosphere. The suspension was filtered and saturated aqueous KPF_6 solution (5 mL) was added to the filtrate, after which a precipitate formed. This precipitate was filtered, washed with water (2 x 20 mL) and dried under vacuo to obtain the compound as dark brown/ red solid. Yield: 0.68 g, 0.07 90%. **^{1}H NMR** (500 MHz, Acetone) δ 8.52 – 8.39 (m, 3H), 8.34 (dd, J = 7.9, 0.9 Hz, 1H), 8.19 (t, J = 8.0 Hz, 1H), 7.90 (d, J = 8.3 Hz, 1H), 7.80 (d, J = 8.8 Hz, 1H), 7.68 (dd, J = 7.9, 1.6 Hz, 1H), 7.15 (d, J = 8.9 Hz, 1H), 7.11 (d, J = 6.2 Hz, 1H), 6.91 (t, J = 7.4 Hz, 1H), 6.38 – 6.30 (m, 1H), 4.61 (d, J = 6.8 Hz, 1H), 4.44 (s, 1H), 1.10 (dd, J = 6.5, 4.1 Hz, 3H). **^{13}C NMR** (126 MHz, Acetone) δ 156.77 (Cq), 155.49 (Cq), 153.76 (CH), 152.49 (Cq), 149.83 (Cq), 147.82 (Cq), 138.46 (CH), 136.43 (CH), 127.54 (CH), 127.24 (CH), 126.95 (CH), 124.48 (Cq), 123.94 (CH), 121.56 (CH), 117.44 (CH), 115.68 (CH), 115.48 (CH), 65.73, 65.68, 23.08 (CH_3). **HR-MS** [M-2(PF_6)]$^{2+}$: 394.10808 (calculated) 394.10743 (measured). **Elem. Anal.** Calcd. For [$C_{42}H_{38}F_{12}N_8O_2P_2Ru$] + 0.2 KPF_6: C, 45.26; H, 3.44; N, 10.05. Found: C, 45.54; H, 3.31; N, 9.36.

3.4.1.6 [6]Cl

The ligand OMe-H_2bapbpy (0.16 g, 0.41 mmol) and [Ru$(DMSO)_4(Cl)_2$] (0.20 g, 0.41 mmol) were added to a flask containing deoxygenated EtOH (25 mL). The solution was refluxed over the weekend at 85 °C under N_2 atmosphere. Afterwards the mixture was

concentrated in vacuo and re-precipitated from MeOH (10 mL) and an excess of diethyl ether (50 mL), filtered and washed with diethyl ether (2 x 50 mL) and dried overnight in vacuo to obtain [**6**]Cl as an orange red solid. Yield: 0.21 g, 0.37, 84%.
^{1}H NMR (500 MHz, DMSO) δ 11.92 (s, 1H), 8.46 (d, J = 7.2 Hz, 1H), 8.37 (d, J = 7.0 Hz, 1H), 8.22 (dd, J = 8.4, 7.8 Hz, 1H), 8.12 (dt, J = 9.3, 8.2 Hz, 2H), 7.98 (t, J = 8.0 Hz, 1H), 7.69 (d, J = 7.5 Hz, 1H), 7.64 (d, J = 7.6 Hz, 1H), 7.39 – 7.32 (m, 2H), 7.14 (d, J = 7.0 Hz, 1H), 6.93 (d, J = 6.8 Hz, 1H), 3.75 (s, 3H), 2.53 (s, 3H), 2.40 (s, 3H). **^{13}C NMR** (126 MHz, DMSO) δ 156.46 (Cq), 156.15 (Cq), 155.07 (Cq), 154.82 (Cq), 154.26 (Cq), 154.07 (Cq), 149.29 (Cq), 148.69 (Cq), 140.86 (CH), 140.07 (CH), 137.69 (CH), 137.27 (CH), 116.90 (CH), 116.54 (CH), 115.56 (CH), 114.19 (CH), 112.31 (CH), 109.03 (CH), 108.22 (CH), 104.74 (CH), 44.55 (CH3), 43.83 (CH3), 43.31 (CH3). **HRMS** $[M+MeCN–2Cl-H]^{+}$: 588.07510 (calculated) 588.07561 (measured). **Elem. Anal**. Calcd. For $[C_{23}H_{22}Cl_2N_6O_2RuS]$ + 1.4 H_2O: C, 42.91; H, 3.88; N, 13.06. Found: C, 42.88; H, 3.64; N, 12.96.

3.4.1.7 [7]Cl

[**6**]Cl (0.11 g, 0.17 mmol) and (R)-methyl p-tolylsulfoxide MTSO (0.54 g, 3.5 mmol) were added to degassed methanol (25 mL). The solution was refluxed for 3 days at 75 °C under N_2 atmosphere. The reaction mixture was concentrated in vacuo and ethyl acetate (10 mL) was added. The suspension was then sonicated for 20 min at room temperature in a Brandson 3510 ultrasonic cleaner. The suspension was filtered and the solid fraction was dried overnight in vacuo to obtain the title compound as yellow solid. Yield: 0.10 mg, 0.15 mmol, 87 %. **^{1}H NMR** (500 MHz, DMSO) δ 8.40 (d, J = 7.9 Hz, 1H), 8.37 – 8.29 (m, 2H), 8.23 (d, J = 7.7 Hz, 1H), 8.19 – 8.01 (m, 6H), 7.98 (t, J = 8.0 Hz, 1H), 7.92 (t, J = 8.0 Hz, 1H), 7.59 – 7.45 (m, 5H), 7.39 (d, J = 7.9 Hz, 1H), 7.33 (d, J = 8.3 Hz, 1H), 7.26 (t, J = 9.1 Hz, 2H), 7.12 (d, J = 8.0 Hz, 1H), 7.11 – 6.98 (m, 6H), 6.93 (d, J = 7.9 Hz, 1H), 6.81 (d, J = 7.8 Hz, 1H), 6.64 (d, J = 8.0 Hz, 2H), 6.58 (d, J = 8.0 Hz, 2H), 3.63 (s, 3H), 3.54 (s, 3H), 2.90 (s, 3H), 2.78 (s, 3H), 2.70 (s, 2H), 2.54 (s, 1H), 2.37 (s, 2H), 2.24 (d, J = 2.5 Hz, 6H). **HR-MS** $[M-Cl]^{+}$: 664.10707 (calculated) 664.10640 (measured). **Elem. Anal**. Calcd. For $[C_{29}H_{26}Cl_2N_6O_2RuS]$ + 0.5 H_2O: C, 49.50; H, 3.87; N, 11.94. Found: C, 48.93; H, 3.71; N, 12.17.

3.4.1.8 [8](Cl)$_2$

The ligand OMe-H_2bapbpy (71 mg, 0.18 mmol) and [Pd(1,5-Cyclooctadiene)$(Cl)_2$] (50 mg, 0.18 mmol) were added to 1-necked-round-bottom flask containing deoxygenated EtOH (25 mL). The solution was refluxed over the weekend at 85 °C under N2 atmosphere. To ensure no side product were removed the reaction mixture was concentrated in vacuo and afforded in [**8**]$(Cl)_2$ in quantitative yield. **^{1}H NMR** (500 MHz, DMSO) δ 12.98 (s, 1H), 8.28 (dd, J = 8.5, 7.6 Hz, 1H), 8.18 (d, J = 6.6 Hz, 1H), 8.13 (t, J = 8.1 Hz, 1H), 7.88 (d, J = 7.4 Hz, 1H), 7.45 (d, J = 7.2 Hz, 1H), 6.72 (d, J = 7.3 Hz, 1H), 3.41 (s, 3H). **^{13}C NMR** (126 MHz, DMSO) δ 163.17 (Cq), 154.24 (Cq), 146.79 (Cq), 146.13 (Cq), 143.88 (CH), 141.64

(CH), 117.22 (CH), 116.12 (CH), 107.01 (CH), 98.87 (CH), 56.62 (CH_3). **ES-MS** $[M\text{-}2Cl\text{-}H]^+$: 505.0 (calculated) 504.9 (measured).

3.4.1.9 [9](Cl)

The ligand OMe-H_2bapbpy (96 mg, 0.24 mmol) and $[Rh(Cl)_3]3H_2O$ (50 mg, 0.19 mmol) were added to 1-necked-round-bottom flask containing deoxygenated EtOH (25 mL). The solution was refluxed over the weekend at 85 °C under N_2 atmosphere. To ensure no side products were removed, the reaction mixture was concentrated in vacuo and was analysed without further purification and afforded $[Rh(OMe\text{-}H_2bapbpy)(Cl)_2]Cl$ in quantitative yield. **^{1}H NMR** (500 MHz, DMSO) δ 11.80 (s, 1H), 8.31 (d, J = 7.6 Hz, 1H), 8.20 (t, J = 8.0 Hz, 1H), 8.03 (t, J = 8.1 Hz, 1H), 7.59 (d, J = 8.4 Hz, 1H), 7.18 (d, J = 8.0 Hz, 1H), 6.65 (d, J = 8.2 Hz, 1H), 3.40 (s, 3H). **ES-MS** $[M\text{-}Cl]^+$: 573.0 (calculated) 572.9 (measured).

3.5 Literature

(1) Havrylyuk, D.; Stevens, K.; Parkin, S.; Glazer, E. C. Toward Optimal Ru(II) Photocages: Balancing Photochemistry, Stability, and Biocompatibility Through Fine Tuning of Steric, Electronic, and Physiochemical Features. *Inorg. Chem.* **2020**, *59* (2), 1006–1013.

(2) Hachey, A. C.; Havrylyuk, D.; Glazer, E. C. Biological Activities of Polypyridyl-Type Ligands: Implications for Bioinorganic Chemistry and Light-Activated Metal Complexes. *Biocatal. Biotransformation Bioinorg. Chem.* **2021**, *61*, 191–202.

(3) Lifshits, L. M.; III, J. A. R.; Ramasamy, E.; Thummel, R. P.; Cameron, C. G.; McFarland, S. A. Ruthenium Photosensitizers for NIR PDT Require Lowest-Lying Triplet Intraligand (3IL) Excited States. *J. Photochem. Photobiol.* **2021**, *8*, 100067.

(4) Busemann, A.; Flaspohler, I.; Zhou, X.-Q.; Schmidt, C.; Goetzfried, S. K.; van Rixel, V. H. S.; Ott, I.; Siegler, M. A.; Bonnet, S. Ruthenium-Based PACT Agents Based on Bisquinoline Chelates: Synthesis, Photochemistry, and Cytotoxicity. *JBIC J. Biol. Inorg. Chem.* **2021**, *26* (6), 667–674.

(5) Zhou, X.-Q.; Busemann, A.; Meijer, M. S.; Siegler, M. A.; Bonnet, S. The Two Isomers of a Cyclometallated Palladium Sensitizer Show Different Photodynamic Properties in Cancer Cells. *Chem. Commun.* **2019**, *55* (32), 4695–4698.

(6) Nano, A.; Dai, J.; Bailis, J. M.; Barton, J. K. Rhodium Complexes Targeting DNA Mismatches as a Basis for New Therapeutics in Cancers Deficient in Mismatch Repair. *Biochemistry* **2021**, *60* (26), 2055–2063.

(7) Scarpantonio, L.; Cotton, S. A.; Del Giorgio, E.; McCallum, M.; Hannon, M. J.; Pikramenou, Z. A Luminescent Europium Hairpin for DNA Photosensing in the Visible, Based on Trimetallic Bis-Intercalators. *J. Inorg. Biochem.* **2020**, *209*, 111119.

(8) Rosenberg, B.; Van Camp, L.; Krigas, T. Inhibition of Cell Division in Escherichia Coli by Electrolysis Products from a Platinum Electrode. *Nature* **1965**, *205* (4972), 698–699.

(9) Cohen, S. M.; Lippard, S. J. Cisplatin: From DNA Damage to Cancer Chemotherapy. In *Progress in Nucleic Acid Research and Molecular Biology*; Academic Press, **2001**; Vol. 67, pp 93–130.

(10) Caballero, A. B.; Cardo, L.; Claire, S.; Craig, J. S.; Hodges, N. J.; Vladyka, A.; Albrecht, T.; Rochford, L. A.; Pikramenou, Z.; Hannon, M. J. Assisted Delivery of Anti-Tumour Platinum Drugs Using DNA-Coiling Gold Nanoparticles Bearing Lumophores and Intercalators: Towards a New Generation of Multimodal Nanocarriers with Enhanced Action. *Chem. Sci.* **2019**, *10* (40), 9244–9256.

(11) Hooper, C. A. J.; Cardo, L.; Craig, J. S.; Melidis, L.; Garai, A.; Egan, R. T.; Sadovnikova, V.; Burkert, F.; Male, L.; Hodges, N. J.; Browning, D. F.; Rosas, R.; Liu, F.; Rocha, F. V.; Lima, M. A.; Liu, S.; Bardelang, D.; Hannon, M. J. Rotaxanating Metallo-Supramolecular Nano-Cylinder Helicates to Switch DNA Junction Binding. *J. Am. Chem. Soc.* **2020**, *142* (49), 20651–20660.

(12) Kelland, L. The Resurgence of Platinum-Based Cancer Chemotherapy. *Nat. Rev. Cancer* **2007**, *7* (8), 573–584.

(13) Armstrong, D. W.; Yu, J.; Cole, H. D.; McFarland, Sherri. A.; Nafie, J. Chiral Resolution and Absolute Configuration Determination of New Metal-Based Photodynamic Therapy Antitumor Agents. *J. Pharm. Biomed. Anal.* **2021**, *204*, 114233.

(14) Lameijer, L. N.; van de Griend, C.; Hopkins, S. L.; Volbeda, A.-G.; Askes, S. H. C.; Siegler, M. A.; Bonnet, S. Photochemical Resolution of a Thermally Inert Cyclometalated Ru(Phbpy)(N–N)(Sulfoxide)+ Complex. *J. Am. Chem. Soc.* **2019**, *141* (1), 352–362.

(15) Li, Y.; Liu, X.; Tan, L. Chiral Ruthenium(II) Complexes as Stabilizers for an RNA Triplex: In Contrast to Λ-Enantiomer, Δ-Enantiomer Stabilizes the Watson-Crick Duplex and the Hoogsteen Strand without Significant Preference. *Dyes Pigments* **2021**, *192*, 109406.

(16) Spence, P.; Fielden, J.; Waller, Zoë. A. E. Beyond Solvent Exclusion: I-Motif Detecting Capability and an Alternative DNA Light-Switching Mechanism in a Ruthenium(II) Polypyridyl Complex. *J. Am. Chem. Soc.* **2020**, *142* (32), 13856–13866.

(17) Boyle, K. M.; Barton, J. K. A Family of Rhodium Complexes with Selective Toxicity toward Mismatch Repair-Deficient Cancers. *J. Am. Chem. Soc.* **2018**, *140* (16), 5612–5624.

(18) Zeglis, B. M.; Pierre, V. C.; Kaiser, J. T.; Barton, J. K. A Bulky Rhodium Complex Bound to an Adenosine-Adenosine DNA Mismatch: General Architecture of the Metalloinsertion Binding Mode. *Biochemistry* **2009**, *48* (20), 4247–4253.

(19) Jackson, B. A.; Barton, J. K. Recognition of DNA Base Mismatches by a Rhodium Intercalator. *J. Am. Chem. Soc.* **1997**, *119* (52), 12986–12987.

(20) Fairbanks, S. D.; Robertson, C. C.; Keene, F. R.; Thomas, J. A.; Williamson, M. P. Structural Investigation into the Threading Intercalation of a Chiral Dinuclear Ruthenium(II) Polypyridyl Complex through a B-DNA Oligonucleotide. *J. Am. Chem. Soc.* **2019**, *141* (11), 4644–4652.

(21) Friedman, A. E.; Chambron, J. C.; Sauvage, J. P.; Turro, N. J.; Barton, J. K. A Molecular Light

Switch for DNA: Ru(Bpy)2(Dppz)2+. *J. Am. Chem. Soc.* **1990**, *112* (12), 4960–4962.

(22) Lim, M. H.; Song, H.; Olmon, E. D.; Dervan, E. E.; Barton, J. K. Sensitivity of Ru(Bpy)2dppz2+ Luminescence to DNA Defects. *Inorg. Chem.* **2009**, *48* (12), 5392–5397.

(23) Saleh, N.; Shen, C.; Crassous, J. Helicene-Based Transition Metal Complexes: Synthesis, Properties and Applications. *Chem. Sci.* **2014**, *5* (10), 3680–3694.

(24) Dhbaibi, K.; Favereau, L.; Crassous, J. Enantioenriched Helicenes and Helicenoids Containing Main-Group Elements (B, Si, N, P). *Chem. Rev.* **2019**, *119* (14), 8846–8953.

(25) Isla, H.; Crassous, J. Helicene-Based Chiroptical Switches. *Emerg. Chem. Fr.* **2016**, *19* (1), 39–49.

(26) Caronna, T.; Mele, A.; Famulari, A.; Mendola, D.; Fontana, F.; Juza, M.; Kamuf, M.; Zawatzky, K.; Trapp, O. A Combined Experimental and Theoretical Study on the Stereodynamics of Monoaza[5]Helicenes: Solvent-Induced Increase of the Enantiomerization Barrier in 1-Aza-[5]Helicene. *Chem. – Eur. J.* **2015**, *21* (40), 13919–13924.

(27) Laarhoven, W. H.; Peters, W. H. M.; Tinnemans, A. H. A. Chirality and Conformational Changes in 4-Phenylphenanthrenes and 1-Phenylbenzo[c]Phenanthrene Derivatives. *Tetrahedron* **1978**, *34* (6), 769–777.

(28) Isla, H.; Srebro-Hooper, M.; Jean, M.; Vanthuyne, N.; Roisnel, T.; Lunkley, J. L.; Muller, G.; Williams, J. A. G.; Autschbach, J.; Crassous, J. Conformational Changes and Chiroptical Switching of Enantiopure Bis-Helicenic Terpyridine upon Zn2+ Binding. *Chem. Commun.* **2016**, *52* (35), 5932–5935.

(29) Brandt, J. R.; Wang, X.; Yang, Y.; Campbell, A. J.; Fuchter, M. J. Circularly Polarized Phosphorescent Electroluminescence with a High Dissymmetry Factor from PHOLEDs Based on a Platinahelicene. *J. Am. Chem. Soc.* **2016**, *138* (31), 9743–9746.

(30) Karras, M.; Dąbrowski, M.; Pohl, R.; Rybáček, J.; Vacek, J.; Bednárová, L.; Grela, K.; Starý, I.; Stará, I. G.; Schmidt, B. Helicenes as Chirality-Inducing Groups in Transition-Metal Catalysis: The First Helically Chiral Olefin Metathesis Catalyst. *Chem. – Eur. J.* **2018**, *24* (43), 10994–10998.

(31) Kos, M.; Rodríguez, R.; Storch, J.; Sýkora, J.; Caytan, E.; Cordier, M.; Císařová, I.; Vanthuyne, N.; Williams, J. A. G.; Žádný, J.; Církva, V.; Crassous, J. Enantioenriched Ruthenium-Tris-Bipyridine Complexes Bearing One Helical Bipyridine Ligand: Access to Fused Multihelicenic Systems and Chiroptical Redox Switches. *Inorg. Chem.* **2021**, *60* (16), 11838–11851.

(32) Bonnet, S.; Siegler, M. A.; Costa, J. S.; Molnár, G.; Bousseksou, A.; Spek, A. L.; Gamez, P.; Reedijk, J. A Two-Step Spin Crossover Mononuclear Iron(Ii) Complex with a [HS–LS–LS] Intermediate Phase. *Chem. Commun.* **2008**, No. 43, 5619–5621.

(33) van Rixel, V. H. S.; Moolenaar, G. F.; Siegler, M. A.; Messori, L.; Bonnet, S. Controlling with Light the Interaction between Trans-Tetrapyridyl Ruthenium Complexes and an Oligonucleotide. *Dalton Trans.* **2018**, *47* (2), 507–516.

(34) van Rixel, V. H. S.; Siewert, B.; Hopkins, S. L.; Askes, S. H. C.; Busemann, A.; Siegler, M. A.; Bonnet, S. Green Light-Induced Apoptosis in Cancer Cells by a Tetrapyridyl Ruthenium Prodrug Offering Two Trans Coordination Sites. *Chem. Sci.* **2016**, *7* (8), 4922–4929.

(35) van Rixel, V. H. S.; Busemann, A.; Wissingh, M. F.; Hopkins, S. L.; Siewert, B.; van de Griend, C.; Siegler, M. A.; Marzo, T.; Papi, F.; Ferraroni, M.; Gratteri, P.; Bazzicalupi, C.; Messori, L.; Bonnet, S. Induction of a Four-Way Junction Structure in the DNA Palindromic Hexanucleotide 5'-d(CGTACG)-3' by a Mononuclear Platinum Complex. *Angew. Chem. Int. Ed.* **2019**, *58* (28), 9378–9382.

(36) Zimmer, K. D.; Shoemaker, R.; Ruminski, R. R. Synthesis and Characterization of a Fluxional Re(I) Carbonyl Complex Fac-[Re(CO)3(Dpop')Cl] with the Nominally Tri-Dentate Ligand Dipyrido(2,3-a:3',2'-j)Phenazine (Dpop'). *Inorganica Chim. Acta* **2006**, *359* (5), 1478–1484.

(37) Mitchell, D. K.; Sauvage, J.-P. A Topologically Chiral [2]Catenand. *Angew. Chem. Int. Ed. Engl.* **1988**, *27* (7), 930–931.

(38) Chambron, J.-C.; Sauvage, J.-P.; Mislow, K.; De Cian, A.; Fischer, J. A [2]Catenane and a [2]Rotaxane as Prototypes of Topological and Euclidean Molecular "Rubber Gloves." *Chem. – Eur. J.* **2001**, *7* (19), 4085–4096.

(39) Addison, A. W.; Rao, T. N.; Reedijk, J.; van Rijn, J.; Verschoor, G. C. Synthesis, Structure, and Spectroscopic Properties of Copper(II) Compounds Containing Nitrogen–Sulphur Donor Ligands; the Crystal and Molecular Structure of Aqua[1,7-Bis(N-Methylbenzimidazol-2'-Yl)-2,6-Dithiaheptane]Copper(II) Perchlorate. *J. Chem. Soc. Dalton Trans.* **1984**, No. 7, 1349–1356.

(40) Arcis-Castíllo, Z.; Zheng, S.; Siegler, M. A.; Roubeau, O.; Bedoui, S.; Bonnet, S. Tuning the Transition Temperature and Cooperativity of Bapbpy-Based Mononuclear Spin-Crossover Compounds: Interplay between Molecular and Crystal Engineering. *Chem. – Eur. J.* **2011**, *17* (52), 14826–14836.

(41) Bode, M. L.; Gates, P. J.; Gebretnsae, S. Y.; Vleggaar, R. Structure Elucidation and Stereoselec-

tive Total Synthesis of Pavettamine, the Causal Agent of Gousiekte. *Tetrahedron* **2010**, *66* (11), 2026–2036.